

INFLUENCE OF MANGANESE ON STRUCTURAL, DIELECTRIC AND MAGNETIC PROPERTIES OF ZnO NANOPARTICLES

T. IQBAL^a, S. GHAZAL^a, S. ATIQ^b, N. R. KHALID^a, A. MAJID^a,
S. AFSHEEN^d, N.A. NIAZ^{c*}

^a*Department of Physics, Faculty of Science, University of Gujrat, Hafiz Hayat Campus, Gujrat, 50700, Pakistan*

^b*Center of Excellence in Solid State Physics, University of the Punjab, Lahore, Pakistan.*

^c*Department of Physics, Bahauddin Zakariya University, Multan, Pakistan*

^d*Department of Zoology, Faculty of Science, University of Gujrat, Hafiz Hayat Campus, Gujrat, 50700, Pakistan*

Pure and Mn doped (1%, 2%, 3% and 4%) zinc oxide (ZnO) nanoparticles had been synthesized by sol-gel auto-combustion method at 300° C. The morphological, structural, dielectric and magnetic properties were analyzed by scanning electron microscope (SEM), X-ray diffractometer (XRD), precession impedance analyzer and vibrating sample magnetometer (VSM) respectively. Hexagonal wurtzite structure was confirmed by XRD and average crystalline size of nanoparticles found to be in the range of 100 nm observed by SEM photographs which shows the decrease in particle size by increasing doping of Mn due to decrease in agglomeration process. Dielectric properties were studied by precession impedance analyzer, which confirmed the decrease in dielectric properties of ZnO by increasing Mn concentration. Characterization of magnetization at room temperature was confirmed in doped ZnO nanoparticles by VSM analysis. Increasing Mn concentration tends to increase the saturation magnetization upto 2% Mn doping and further increase in dopant concentration dramatically decreased the saturation magnetization which shows that Mn concentration beyond 2% convert the magnetic behavior from ferromagnetic to paramagnetic.

(Received June 9, 2016; Accepted August 19, 2016)

Keywords: Mn-doped ZnO, Sol-gel, Morphology, VSM, Dielectric properties

1. Introduction

Formation of semiconductor nanostructures and their industrial use has attracted much attention of scientists from the last few decades due to their novel electronic, optical and photonic device applications [1], [2] such as schottky diode, display technology, MESFET and transparent integrated circuits. Zinc oxide (ZnO) is II-VI n-type semiconductor which has a wurtzite crystal structure [3] and having a direct band gap of 3.37 eV [4]. It has specific and unique properties such as high electron mobility, high thermal conductivity and wide band gap which makes ZnO a potential candidate for its applications in various electronic devices [5] such as Seo *et al* studied the field effect transistor based on ZnO nanoparticles [6] and a light controlling, flexible gas sensor was fabricated by Zheng *et al* using commercial ZnO nanoparticles [7]. Apart from its applications in electronic devices ZnO is also used in ceramics, pharmaceuticals, agriculture etc. [8]. Doping of transition metals in ZnO surprisingly changes its properties but its structure remains same. This dramatic change in different properties of ZnO such as high dielectric constant, magnetic strength and other high technology applications, which have not commercial reality yet, attract the researchers to enhance its properties [9]. This change in properties of ZnO has open new doors toward research and electronic devices which have been investigated earlier

*Corresponding author: niazpk80@bzu.edu.pk

[10]-[13]. Transition metal (such as manganese) doped ZnO is synthesized and characterized in order to understand the unique and tremendous properties and to explore the applications of DMS.

The particular study of doping into nanoparticles and dramatic effect of dopant on the properties of ZnO based nanoparticles seeking more attention towards the research. [14] The diluted magnetic semiconductor (DMS) nanostructures, which are well known for their spintronic property, [15]-[17] have attracted great interest of researchers. Most fascinating property of DMS is that doping of magnetic material into semiconductors do not affect crystal structure but dramatically changes its dielectric and magnetic properties i.e. room temperature ferromagnetism is observed in transition metal doped ZnO [18] [19]. DMS are synthesized by doping of a small amount of transition metal such as Cr, Ni, Mn, Co or Fe in semiconductor material such as ZnO [20] which improves and enhances the structural, dielectric and magnetic properties of pure semiconducting material as compared to undoped nanoparticles.

When transition metal, such as manganese, is induced in ZnO, it replaces Zn atoms and electrons are the charge carriers i.e. electrons have an additional property of spin along with charge, which causes the magnetism in ZnO. Due to this unique property of DMS, they are used where ferromagnetism is required in the semiconductor devices. The charge carriers in such devices give the data processing and magnetic storage in a single chip. Furthermore, DMS materials are also used to make novel devices such as spin transistors for mobile applications, optical emitters and integrated magnetic/electronic devices. Interestingly, Mn doping also changes the dielectric properties of ZnO, such as dielectric constant, loss factor and tangent loss dramatically reduces by Mn doping into ZnO. Therefore dielectric measurements are used to study the dynamic properties such as dielectric constant, conductance, inductance, capacitance, impedance, loss factor and tangent loss of the material. Such materials, having high dielectric properties, are expeditiously using in dynamic applications of microelectronics, gas sensors, and transparent conducting electrodes etc. [21].

In this paper, pure and Mn doped ZnO nano particles are synthesized by using sol-gel auto-combustion method, combusted at 300° C. This method is preferred due to the reason that it is less energy consuming, less time consuming and low cost approach. Amount of dopant is taken as 1, 2, 3 and 4 percent. Structural, dielectric, morphological and magnetic properties are analyzed and discussed. This is unique study which investigates the properties such as dielectric constant, morphology and magnetic behavior which show a remarkable change by doping the transition metal such as Mn in ZnO.

2. Materials and methods

2.1 Synthesis

The process of chemical synthesis with direct combustion for doped ZnO gives better composition control over the materials. [22] For this purpose, sol-gel auto combustion method is selected. This is a beneficial process as all the impurities kindle during the synthesis process and there is no need to purify the sample again and again. The precursors and their composition used for this method is unique and never used before. Pure and manganese substituted ZnO were synthesized by sol-gel auto combustion method. Pure ZnO was prepared by mixing the citric acid $C_6H_8O_7$ and zinc nitrate hexa-hydrate $[Zn(NO_3)_2 \cdot 6H_2O]$ in 75ml of de-ionized water. After the stirring of 3 hours at ~80 °C which converted this solution to gel, which was further heated at 250 °C. Gel was ignited to convert it into ash which was grinded and calcinated at 300 °C for 6 hours. Mn doped ZnO was produced by magnetic stirring the solution of zinc nitrate, manganese nitrate $[Mn(NO_3)_2 \cdot 4H_2O]$ and citric acid soluble in de-ionized water. The same protocol was used as mentioned above for pure ZnO. Various amounts of $[Mn(NO_3)_2 \cdot 4H_2O]$ are used for different doping concentration.

2.2 Characterization

The powders of pure ZnO nanoparticles and doped with Mn were characterized by various techniques to determine different properties i.e. crystal structure and morphology of Mn doped ZnO nano-composites were characterized by using X-ray diffraction (XRD) technique. Dielectric

properties were studied by precession impedance analyzer. Scanning electron microscope (SEM) was used to study the material composition of nano-particles. Magnetic properties were discussed by using vibrating sample magnetometer (VSM).

3. Results and discussion

3.1 Scanning electron microscopy

The scanning electron microscopic figures of pure and Mn doped ZnO are taken within the range of 100nm with magnification of 50,000x, at an accelerating voltage of electron beam of 50 kV which are shown in Fig.1. Image show that particles are spherical in shape and are in the range of 20-40 nm. Particle agglomeration is also observed in topical view of SEM image for pure ZnO as shown in Fig.1 (A).

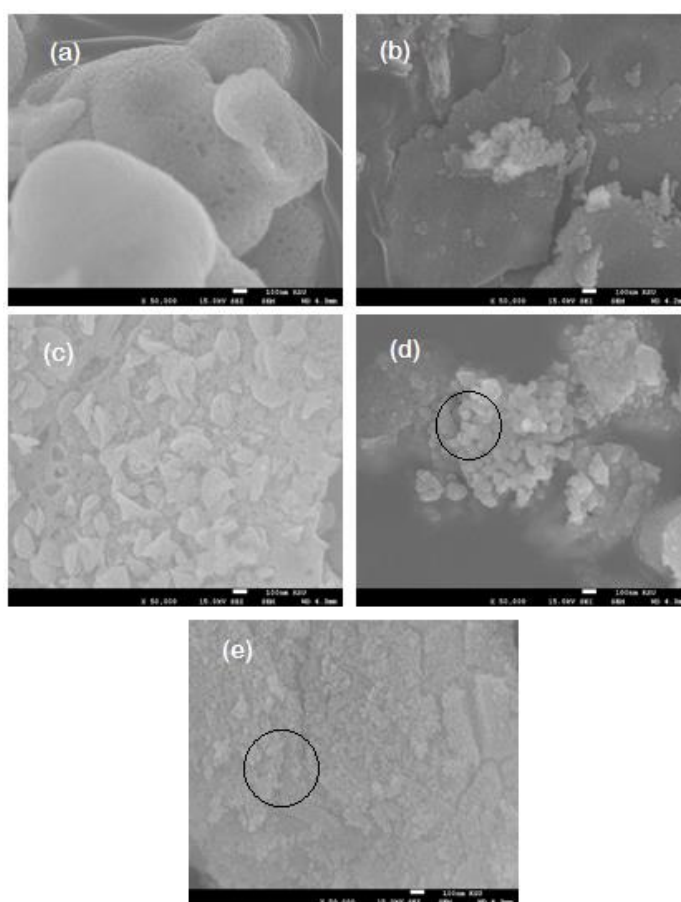


Fig. 1. SEM Nano graph of pure and Mn doped ZnO. (a) Pure ZnO, (b) 1% Mn doped ZnO, (c) 2% Mn doped ZnO, (d) 3% Mn doped ZnO and (e) 4% Mn doped ZnO. Encircled region shows uniformly distributed particles

Pure ZnO has greater particle size while the doping of Mn tends to decrease the particle size as the doping of 1% Mn also shows the agglomeration due to the lesser amount of Mn doping, 2% Mn doped nanoparticles shows less agglomeration and 3% and 4% Mn doped ZnO nanoparticles are uniformly distributed. The results show that as the doping increases agglomeration process decreases and particles uniformly distributed [23]. In addition, highly doped ZnO particles are spherical in shape and are closely arranged with each other. Even though, the clear boundary between the particles is observed which distinguish them, this is shown in encircled region of Fig. 1(d) and (e).

3.2 X-ray diffraction

Diffraction patterns of pure and (1- 4%) Mn doped ZnO nanoparticles of XRD is determined in Fig.2. The diffraction peaks have orientations as (100), (002), (101), (102), (110), (103) and (201) which are calculated by the Brag's formula. [24]

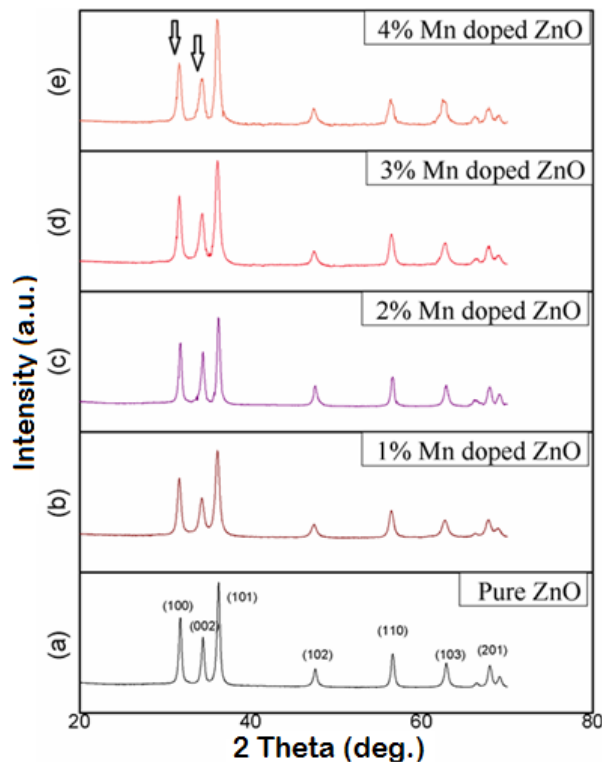


Fig. 2. X-ray diffraction patterns for pure and Mn doped ZnO.

The peaks clearly show hexagonal wurtzite structure for all the samples. The comparison of XRD of all the samples show that there is a trivial shift in first three peaks of samples which are doped with Mn in comparison to pure ZnO which confirms the doping of Mn into ZnO samples. All the patterns have no extra peak or any fluctuation which means that doping has no effect on structure of ZnO and the dopant i.e. Mn is uniformly distributed over the whole surface of ZnO replacing the zinc ions as shown in Fig.2. Furthermore, no extra peak is observed in the data which confirms the absence of any impurity in the crystal. Fig.2 depicts that first two diffraction peaks (110) and (002) Mn doped ZnO nanoparticles show a trivial shift of 0.20° towards the lower angle with reference to pure ZnO. This shift is due to the replacement of Mn ions, at tetrahedral sites of crystal lattice, which are larger than Zn ions [25].

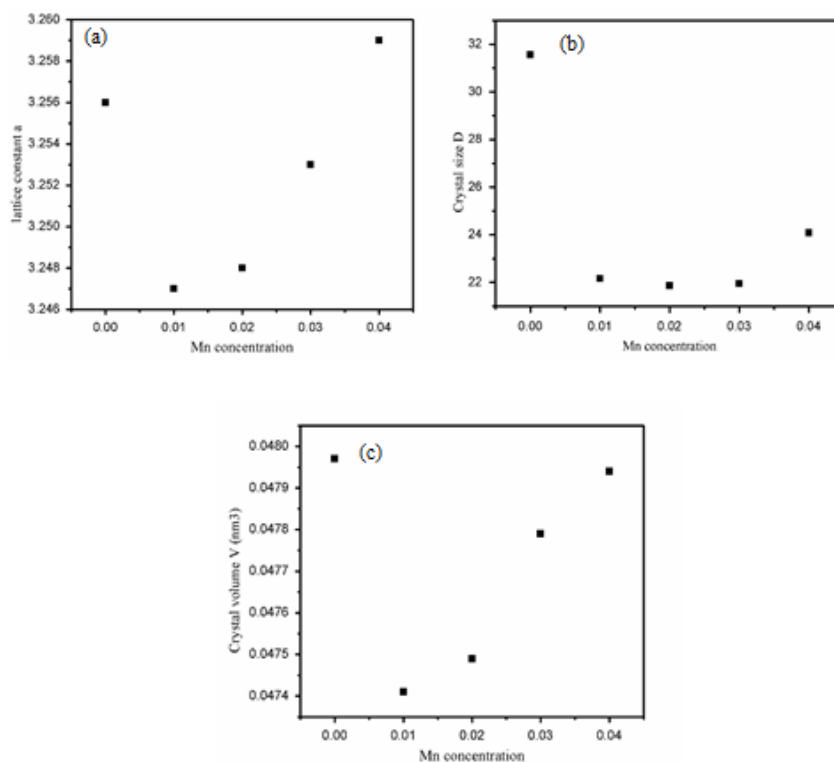


Fig. 3. Variation of crystal parameters, (a) lattice parameter, (b) crystal size, (c) volume, by varying Mn concentration.

Value of lattice parameter 'a' for pure ZnO is calculated as $a = 3.247 \text{ \AA}$ and lattice parameter 'c' is $c = 5.202 \text{ \AA}$ by Bragg's formula. All these peaks are in accordance with JDCPS Card no. 36-1451 [26]. Similarly, lattice parameters for Mn doped ZnO are also calculated which are given in Table.1 along with crystal size and volume of ZnO crystal which clearly shows that lattice constants 'a and c' decreases by doping Mn into ZnO and increases linearly by increasing doping concentration of Mn which is another evidence of Mn substitution in ZnO crystal which is also reported in literature [21], [23], [27] this is also shown in Fig. 3(a).

Table 1: calculated value of lattice constants, crystal size and volume of pure and Mn doped ZnO from XRD data.

Mn content	a (Å)	c (Å)	FWHM (β)	Crystal size D (nm)	Volume V (nm ³)
x = 0.00	3.256	5.202	0.46259	31.557	0.04749
x = 0.01	3.247	5.225	0.65782	22.161	0.04797
x = 0.02	3.248	5.19	0.6669	21.866	0.04741
x = 0.03	3.253	5.216	0.6643	21.946	0.04779
x = 0.04	3.259	5.213	0.60535	24.079	0.04794

This variation of lattice parameters is due to larger radius of replaced Mn ion than the Zn ion. This may be explained by the Vegard's law as which explains that the difference in lattice constants of undoped and doped ZnO are due to difference in lattice parameters of Mn and ZnO and lattice constant of ZnO increases by increasing the doping concentration of Mn as predicted by Vegard's law. [28] Fig. 3(b) represents the crystal size of nanoparticles which shows greater value of pure zinc oxide and sudden decrease in values after doping. A microstrain is induced in the ZnO nanoparticles due to the doping of Mn, which has a larger radius than Zn, which disturb the grain growth process and particle size reduces. Volume also varies by changing Mn concentration which is represented in Fig. 3(c) and are in good agreement with the values reported by Anghei *et al.* [29]

which is given in the range of 0.04754 to 0.0478 nm³ and also with values of Y. Koseoglu [23] which has reported the range of 0.0474 to 0.0476 nm³.

The value of bulk density (ρ_b), X-ray density (ρ_x) and porosity (P) of material is also calculated from XRD data which is given in Table 2. Bulk density and X-ray density show the decreasing trend by increasing Mn concentration while porosity increases by increasing dopant in ZnO.

Table 2. Calculated values of bulk density (ρ_b), X-ray density (ρ_x) and porosity (P) of material

Parameter	$x = 0$	$x = 0.01$	$x = 0.02$	$x = 0.03$	$x = 0.04$
Bulk density (g/cm ³)	2.66	2.459	2.536	2.5	2.45
X-ray density (g/cm ³)	5.96	5.636	5.702	5.657	5.639
Porosity	0.533	0.563	0.555	0.558	0.565

3.3 Dielectric measurements

The behavior of Dielectric properties of ZnO i.e. dielectric constant, loss factor and tangent loss is studied by precession impedance analyzer. Dielectric properties are the function of frequency and changes by varying applied frequency signal. Dielectric constant is a significant property which affects many optoelectronic and transport properties of material [30]. Dielectric constant of pure ZnO is maximum for low frequency and is observed to be exponentially decreased by increasing frequency. This behavior can be explained by Maxwell-Wagner model [31] according to which material is composed of grains, which are well conducting, and separated by grain walls, which are poor conducting. When external field is applied, charge carriers move freely within grains and accumulate at grain boundary. At low frequency, charge carriers do not diffuse from grain boundary as the accumulation is very high. But at higher frequency, charge carriers do not follow the applied field due to accumulated charge carriers within the grain, which decreases the dielectric constant.

Doping also affect the dielectric properties as the doping of Mn decreases the dielectric constant of ZnO at the same frequency. This causes the maximum value of dielectric constant to reduce at constant frequency as shown in Fig.4 (a).

This is due to the fact that doping of cation i.e. Mn⁺³ affect the polarizability of ZnO [32] i.e. Mn ion neutralizes the oxygen ion and reduces the dipoles within the crystal. Thus, polarizability lags behind the applied field as frequency increases and the same trend is observed for tangent loss and loss factor shown in Fig. 4 (b) and (c). Tangent loss is the measure of loss of energy into the sample when field is applied. This decreasing trend indicates that a microstructure is formed with ZnO grains which not only surround the grain boundaries but also cause an interface state in grain boundaries. Hence, the samples show dielectric dispersion which is high at low frequency and exponentially decreases as the frequency increases. At higher frequencies it almost become frequency independent which is clearly been observed from Fig.4(c).

This phenomenon is well explained by Koop's phenomenological theory [33] according to which, it is assumed that material is made of two things. One is grains which are well conducting and more effective at higher frequencies while other are grain boundaries which are poorly conducting and more effective at lower frequencies. Charge carriers, which carries the polarization phenomena, lags behind the applied alternative field. Beyond the certain limit of applied frequency, these charges have no effect on the change of applied field. Thus at higher frequencies, all the phenomena of polarization becomes almost frequency independent.

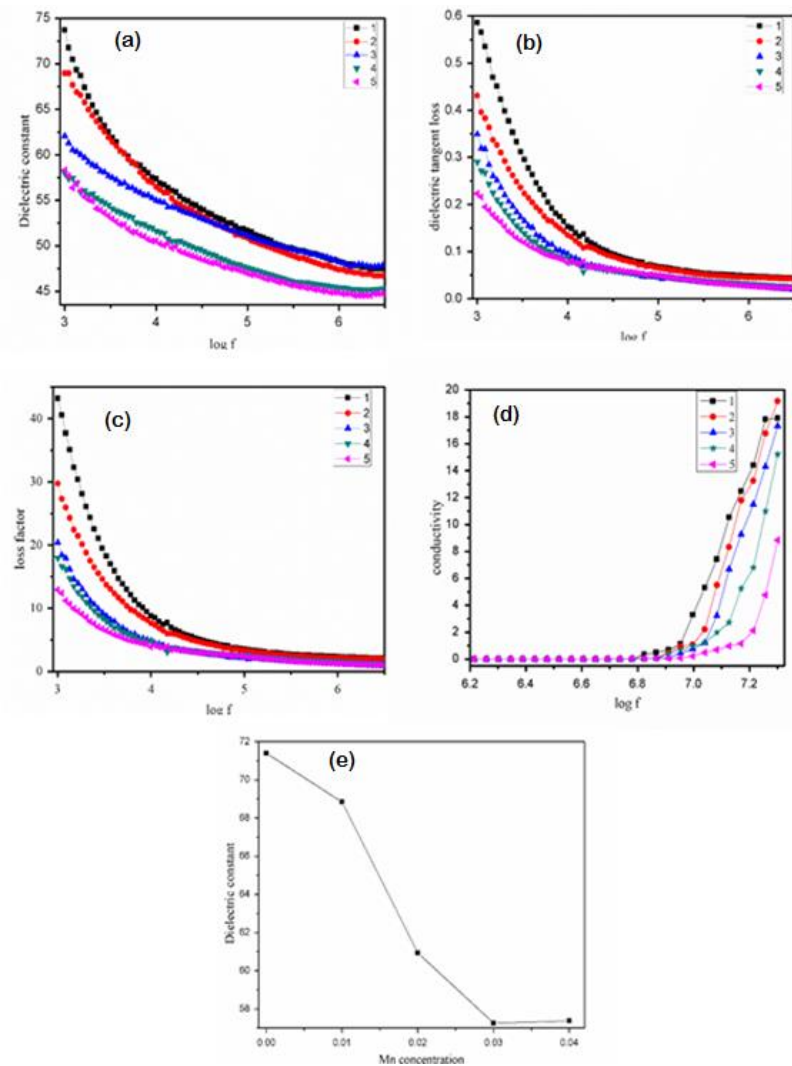


Fig. 4. Variation of dielectric properties by increasing frequency. Variation in (a) dielectric constant, (b) loss factor, (c) tangent loss by changing frequency. (d) Conductivity, (e) Variation in dielectric constant by changing Mn concentration.

Fig.4 (d) indicates the variation of ac conductivity σ_{ac} for pure and Mn doped ZnO nanoparticles characterized at room temperature. Graph shows the exponentially increasing trend of conductivity for pure and Mn doped ZnO by increasing applied ac frequency. Comparison of the conductivity of pure ZnO and Mn doped ZnO clearly shows decreasing trend i.e. pure ZnO shows the curve at higher values of conductivity while doping tend to shift this curve at lower values. It can be attributed to the fact that increasing content of Mn ion (which replaces Zn) increases the donor defects due to which system is diluted. This fact decreases the n-type conductivity of host ZnO. [33]

Fig.4 (e) shows the decreasing trend of dielectric constant by increasing Mn concentration in ZnO. This shows that doping of Mn upto 3% has exponentially decreased the value of dielectric constant while 4% Mn doping doesn't show remarkable difference in dielectric constant. Tangent loss and loss factor also decreases by increasing Mn doping concentration in the same way. M. M. Hassan *et al* [33] and M L Dinesha *et al* [34] also reported the same trend of dielectric properties of transition metal such as Fe doped ZnO nanoparticles but they reported comparatively lower values of dielectric constant and conductivity than Mn doped ZnO.

3.4 Magnetization measurements

Magnetization measurements of pure and Mn doped ZnO nanostructures were characterized at room temperature by using vibrating sample magnetometer (VSM). VSM analysis for undoped ZnO nanostructure show linear behavior at room temperature which indicates the diamagnetic behavior of ZnO nanostructure. The reason is that paired electrons of 2p orbital of oxygen and 3d orbital of zinc combine to form ZnO. No unpaired electron is there to produce ferromagnetism. However room temperature ferromagnetism is also observed in some cases due to the defects [35,36]. On doping the Mn into ZnO nanostructure i.e. from 1% to 4%, ferromagnetism phenomenon is observed by M-H curve as shown in Fig.5.

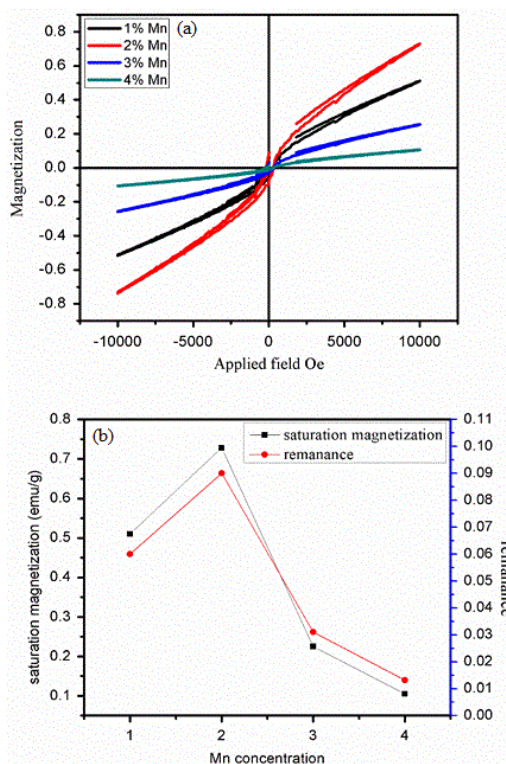


Fig. 5. (a) M-H curve for 1-4% Mn doped ZnO, (b) observed values of saturation magnetization M_s and remanence M_R for M/H curves of Mn doped ZnO where curve on the fig. shows maximum value of M_s .

Magnetization in ZnO nanoparticles is induced by doping of transition metal doping i.e. Mn which replaces the Zn ion on doping. Mn ions have magnetic dipole moment due to spin of unpaired electrons which actually split the band gap of ZnO into two, (1) for spin up electrons and (2) for spin down electrons and one has higher concentration than other. Due to this higher concentration of spinning electrons ferromagnetic exchange interactions occur in Mn ions and oxygen ions that results in the induction of ferromagnetism into ZnO nanoparticles. This exchange interaction is due to overlap of 3d orbital electrons with oxygen vacancies or interstitial Zn atom in ZnO nanoparticles. [37]- [39] Values of magnetic properties are given in Table 3.

Table 3: values of magnetic properties obtained from M/H curve.

Mn concentration	Coercivity (Oe)	Saturation magnetization (emu/g)	Remanence (emu/g)	Squarances ratio
1	327	0.51	0.06	0.117
2	339.5	0.728	0.09	0.1236
3	315.5	0.225	0.031	0.1215
4	303.5	0.105	0.01314	0.125

M-H curves for 1% and 2 % Mn doping indicate that saturation magnetization M_s value increases due to increasing the doping element while further increase of dopant i.e. 3% and 4% tend to decrease the value of saturation magnetization. M. Bououdina *et al* [40] also reported the same trend for ferromagnetism. Maximum value of saturation magnetization is 0.728 emu/g at 339.5 Oe coercivity for 2% doping. It is cleared from Fig. 5(b) that there is a maximum value of M_s (encircled region) at 2% Mn doping and further increase of dopant tend to fall M_s at lower values and the same trend is observed for remanence in M/H curve. This ferromagnetism is due to unpaired electrons of Mn dopant. These results show the increasing trend of ferromagnetism upto 2% doping and further increase of dopant tend to decrease the ferromagnetic behavior in Mn doped ZnO nanoparticles enhancing the paramagnetic component. Decrease in ferromagnetism is due to Antiferromagnetism in higher Mn concentration.

4. Conclusion

In conclusion, pure and Mn doped ZnO nanoparticles with different doping concentrations are prepared by using sol-gel auto-combustion method. SEM images confirms the range of nanoparticles within the range of 20-40 nm. It reveals that doping reduces the agglomeration process and particle size reduces by increasing doping concentration which is also confirmed by calculation of XRD results. XRD analysis confirms that crystal structure of undoped and Mn doped ZnO is hexagonal wurtzite structure. The comparison of XRD of all the samples show the same peaks which means that doping has no effect on structure of ZnO and Mn is uniformly distributed over the whole surface of ZnO but it changes the lattice parameters 'a' and 'c', particle size and volume of crystal due to replacement of Mn from Zn which confirms that Mn has doped into ZnO. Dielectric measurements show that dielectric properties such as dielectric constant, loss factor and tangent loss are the function of frequency and they reduces by increasing the doping concentration due to the reason that doping affect the polarizability of ZnO i.e. some of the Mn ions neutralizes the oxygen ions and reduces the dipoles within the crystal which also confirms that Mn is really induced in ZnO crystal. VSM analysis of pure ZnO confirms no ferromagnetism in nanoparticles. On doping the Mn into ZnO nanostructure i.e. from 1% to 4%, ferromagnetism phenomenon is observed by M-H curve. M-H curves also indicate that saturation magnetization value increases upto 2% Mn doping and further increase of dopant decreases ferromagnetic behavior.

References

- [1] X. Duan, Y. Huang, Y. Cui, J. Wang and C.M. Lieber: Nature **66**, 409 (2001).
- [2] H. M. Huang, S. Mao, H. Feick, H. Yan, H. Wu and H. Kind, Science **292**, 1897 (2001).
- [3] J. Kaur, S. Singhal, Ceramics international, **40**, 7417 (2014).
- [4] D. Zhang, J. Zhang, Z. Guo, X. Miao, Journal of alloys and compound **509**, 5962 (2011)
- [5] A. Janotti, Chris G Van de Walle, Reports on Progress in Physics **72**, 126501, (2009).
- [6] Y. K. Seo, S. Kumar, G. H. Kim, Journal of Nanoscience Nanotechnology **6**, 4852, (2011).

- [7] Z. Q. Zheng, J. D. Yao, B. Wang G. W. Yang, *Scientific Reports* **5**, 11070, (2015).
- [8] A.K. Radzimska, T. Jesionowski, *Materials* **7**, 2833, (2014).
- [9] A. Moezzi, Andrew M. McDonagh, Michael B. Cortie, *Chemical Engineering Journal* **185**, 1 (2012).
- [10] X. Hou, H. Sun, L. Liu, X. Jia, H. Liu, *Journal of Alloys and Compounds* **640**, 444 (2015).
- [11] R.A. Torquato, Sagar E. Shirsath, R.H.G.A. Kiminami, A.C.F.M. Costa, *Ceramics International* **40**, 6553 (2014).
- [12] Y. Mao, S. Ma, X. Li, C. Wang, F. Li, X. Yang, J. Zhu, L. Ma, *Applied Surface Science* **298**, 109 (2014).
- [13] A.I. Savchuk, A. Perrone, A. Lorusso, I.D. Stolyarchuk, O.A. Savchuk, O.A. Shporta, *Applied Surface Science* **302**, 205, (2014).
- [14] G. Murugadoss, "Synthesis and Characterization of Transition Metals Doped ZnO Nanorods", *Journal of Material Science and Technology* **28**(7), 587 (2012).
- [15] J.K. Furdyna, *Journal of Applied Physics* **64**, 29 (1988).
- [16] H. MuneKata, H. Ohno, S. Von Molnár, et al., *Physics Review Letter* **63**, 1849 (1989).
- [17] C. Ronning, P. X. Gao, Y. Ding, and Z. L. Wang, *Applied physics letters* **84**, 783 (2004)
- [18] C. Jing, Y. Jiang, W. Bai, J. Chu, A. Lio, *Journal of magnetism and magnetic materials* **322**, 2395 (2010).
- [19] Y. Jiang, W. Wang, C. Jing, C. Cao, J. Chu, *Material science and Engineering* **176**, 1301 (2011)
- [20] E. Asikuzun, A. Donmez, L. Arda, O. Cakiroglu, O. Ozturk, D. Akcan, M. Tosun, S. Ataoglu, C. Terzioglu, *Ceramics International* **41**, 6326 (2015).
- [21] R. K. Shukla, A. Srivastava, K. C. Dubey, N. Kumar, *International Conference on Emerging Trends in Electronic and Photonic Devices & Systems*, (2009)
- [22] J.Iqbal, X. Liu, A. Majid, R. Yu, *Journal of Superconductivity and Novel Magnetism* **24**, 699 (2011).
- [23] P. Moontragoon, S. Pinitsoontorn, P. Thongbai, *Microelectronic engineering* **108**, 158, (2013).
- [24] Y. Koseoglu, *Ceramics international* **41**, 11655 (2015)
- [25] Xu, H.Y. Liu. Y.C. Xu, C.S. Liu, Y.X. Lhao, C.L.Mu, R.J. Chem, C.L. Mu, R., *Journal of Chemistry and Physics* **124**, 074707 (2006).
- [26] JDCPS card no. 36-1451
- [27] S. Muthukumar R. Gopalakrishnan, *Journal of Material Science: Materials in Electron* **23**, 1393, (2012).
- [28] Y. K. Kou, B. T. Liou, S. H. Yen, H. Y. Chu, *Optics Communications* **237**, 363, (2004).
- [29] J. Anghel, A. Thurber, D.A. Tenne, C.B. Henna, A. Punnoose, *Journal of applied physics*, **107**, 09E314 (2010).
- [30] C. Jayachandriah, G. Krishnaiah, *Advanced Materials Letters*, **10.5185**, 5801 (2015)
- [31] Prodromakis, T.; Papavassiliou, C.; *Applied Surface Science* **255**, 6989 (2009).
- [32] Li H, Huang Y, Zhang Q, Qiao Y, Gu Y, Liu J, Zhang Y, *Nanoscale*, 654, (2011).
- [33] M. M. Hassana, A. S. Ahmeda, M. Chamana, W. Khana, A.H. Naqvia, A. Azam, *Materials Research Bulletin* **47**, 3952 (2012).
- [34] M. L. Dinesha, G. D. Prasanna, C. S. Naveen, H. S. Jayanna, *Indian Journal of Physics* **87**, 147 (2013)
- [35] R. Podila, W. Queen, A.Nath et al., *Nano Lettler* **10**, 1383 (2010).
- [36] B.B. Straumal, A.A. Mazilkin, S.G. Protasova et al., *Physical Review* **B 5**, 8871 (2009).
- [37] J. J. Liu, K. Wang, M. H. Yu, W. L. Zhu, *Journal of applied physics* **102**, 024301, (2007).
- [38] J. D. M. Coey, M. Vankatesan, C. B. Fitzgerald, *Nature materials* **4**(4), 173 (2005).
- [39] M. H. F. Sluiter, Y. Kawazoe, P. Sharma, A. Inove, A. R. Raju, C. Rout, *Physical review letters* **94**, 187204 (2005).
- [40] M. Bououdinaa, K. Omri, M. El-Hilo, A. El Amiri, O.M. Lemine, A. Alyamani, E.K. Hlilg, H. Lassri, L. El Mir, *Physica E* **56**, 107 (2014).